

Numerical Simulations of Unstable Flow through a Spherical Bulge in a 90-degree Asymmetrical Bend

J.M.M. Sousa ¹

Abstract: Time-dependent numerical simulations of the flow through a spherical bulge in a 90-degree asymmetrical bend have been performed for Reynolds numbers in the range 100-400. The present results have demonstrated that the flow reaches asymptotically steady, symmetrical solutions for Reynolds numbers up to 300, whereas a value of 400 for this parameter leads to unsteadiness. The computed flow behavior at this higher Reynolds number has shown to be characterized by an intermittent transition between small-amplitude, irregular oscillations and large-amplitude bursts occurring at a low frequency. In addition, the unsteady flow was asymmetrical and exhibited swirl switching.

keyword: Unstable flow, symmetry-breaking, intermittency, spherical bulge, asymmetrical bend.

1 Introduction

It is well known that impinging jets and flows in cavity-type geometries are prone to exhibit self-sustained oscillations [Rockwell and Naudascher (1978)]. Both periodic [Ghaddar, Korczak, Mikic and Patera (1986); Pereira and Sousa (1993)] and aperiodic cavities [Rockwell (1977); Pereira and Sousa (1995)] have been shown to develop an oscillatory flow behavior when a certain value of the Reynolds number is exceeded. On the other hand, the classical example of a diverging channel (with the sudden expansion as a limit case) is also known to present hydrodynamic instabilities that may lead to different types of bifurcations [Drazin (1999)]. Symmetry-breaking of the flow, giving rise to non-unique solutions, arise in such flows through a supercritical pitchfork bifurcation [Fearn, Mullin and Cliffe (1990); Durst, Pereira and Tropea (1993); Drikakis (1997)]. In addition, transition from a steady solution to periodic flow has been reported to occur in channels with expanded sections as

a consequence of a Hopf bifurcation [Sobey and Drazin (1986); Mizushima, Okamoto and Yamaguchi (1996)].

The flow through a bulge in a bend may be geometrically classified as a cavity-type problem, displaying a three-dimensional, gradual expansion and contraction of the flow along the main channel. Furthermore, the confined jet produced at the entrance of the bulge eventually impinges at the opposite surface, thus providing an additional source of instability in this flow. In fact, impingement-type geometries usually exhibit well-organized oscillation patterns [Rockwell and Naudascher (1979)]. It is widely accepted in the literature that the occurrence of organized phenomena in confined geometries is due to a feedback effect. Initial disturbances convected by the flow interact with the impingement point, producing a feedback that ultimately results in the establishment of a periodic cycle.

The practical interest of the present work can be found in two distinct fields of research: *in vitro* studies of hemodynamics and pharmacokinetics.

Concerning the first application, the relevance of this particular geometry arises from the fact that it can be seen as a simplified model of a saccular aneurysm. Flows through bends display regions where rapid changes in wall shear stresses occur, making such areas of a vessel particularly vulnerable to abnormal biological responses [Ku (1997); Berger and Jou (2000)]. Although a Newtonian fluid was considered here and the effects of compliant walls and pulsatile inlet flow were not taken into account at this stage, the numerical simulations carried out for the present investigation are in the same range of Reynolds number as the blood flow in intracranial arteries [Liou and Liou (1999)]. Studies of hydrodynamic stability [Yip and Yu (2001)], chaotic mixing [Butty, Gudjonsson, Buchel, Makhijani, Ventikos and Poulikakos (2002)] and flow dynamics [Valencia (2004)] in aneurysm models have been reported in the literature, demonstrating the importance of these problems.

¹Instituto Superior Técnico, Technical University of Lisbon, Av. Rovisco Pais, 1049-001 Lisboa, Portugal.

The second application stems from the observation that the present geometry faithfully reproduces the induction port (throat) of a standard apparatus used in the pharmacological assessment of the performance of dry powder inhalers [Hallworth and Westmoreland (1987)]. The device is the basis of one of the widest used reference methods for *in vitro* testing of inhaled aerosols, as described in the various Pharmacopoeias. Compendial methods have the advantage that these have been validated in many laboratories but are often not based on the latest technology [Mitchell and Nagel (1997)], which supports the need for further investigation. In this case, it can be easily demonstrated that the dynamics of the gas flow will have a significant impact on the deposition characteristics of the aerosol in the testing device. The Reynolds numbers of interest for this application are generally higher than those reported for hemodynamic problems, say higher than 1000. However, inspiratory flow rates associated to children or asthmatic patients lead to flows characterized by significantly lower Reynolds numbers.

The present work addresses the unstable behavior exhibited by the flow through a spherical bulge in a 90-degree asymmetrical bend. Time-dependent numerical solutions of the Navier-Stokes equations have been obtained for Reynolds numbers in the range 100-400, employing a finite-volume method. A physical interpretation of the flow dynamics based on the theory of dynamical systems has been provided as well.

2 Numerical formulation

2.1 Governing equations

The mass and momentum conservation equations governing the unsteady flow of an incompressible, Newtonian fluid were solved numerically. Denoting the fluid density by ρ , the velocity vector by \mathbf{v} and the stress tensor by $\boldsymbol{\tau}$, these equations can be written in vector form, independently of the coordinate system, as

$$\nabla \cdot (\rho \mathbf{v}) = 0, \quad (1)$$

$$\frac{\partial}{\partial t} (\rho \mathbf{v}) + \nabla \cdot (\rho \mathbf{v} \otimes \mathbf{v} - \boldsymbol{\tau}) = 0, \quad (2)$$

where the stress tensor, from Stokes' hypothesis, is given by

$$\boldsymbol{\tau} = - \left(p + \frac{2}{3} \mu \nabla \cdot \mathbf{v} \right) \mathbf{i} + \mu (\nabla \mathbf{v} + \nabla^t \mathbf{v}). \quad (3)$$

In Eq. (3) μ is the dynamic viscosity, p is the pressure and \mathbf{i} stands for the unit tensor of second order.

2.2 Discretization procedure and method of solution

Steady and time-dependent flow solutions have been obtained employing the finite-volume method to discretize the equations on a structured, non-orthogonal, non-staggered grid system. The numerical method is second-order accurate in space and in time, using Crank-Nicholson and Adams-Bashforth time-stepping procedures to advance diffusion and convective terms in time, respectively.

Denoting by ϕ_j a generalized dependent variable calculated at a control volume j , the semi-implicit procedure can be expressed as follows:

$$\phi_j^{n+1} = \phi_j^n + \frac{1}{2} (3C_j^n - C_j^{n-1}) + \frac{1}{2} (D_j^{n+1} + D_j^n), \quad (4)$$

where C_j^n and D_j^n are the terms resulting from the application of the discretization procedure to the convective and diffusion parts of the governing equations, respectively, evaluated at time level n . The pressure field is obtained from the solution of a Poisson equation obtained by combining Eqs. (1)-(2). Additional details regarding the numerical method were given by Pereira and Sousa (1999). In the foregoing paper it was also demonstrated that this numerical method has the capability of providing accurate predictions of steady and oscillatory regimes for confined vortex breakdown flows up to $Re = 3100$, employing similar grid resolutions.

In the present case, a 90-degree asymmetric bend exhibiting a spherical bulge with an inlet diameter ratio of 16/9 was considered. The bend is asymmetric because the outlet channel has a smaller diameter than the inlet duct and its axis is displaced by a small amount with respect to the axis of the sphere. The diameter ratio between the two ducts is 35/54 and the ratio of the axis displacement to the main channel diameter is 1/15. The boundaries defining the exact geometry of the physical domain where numerical solutions of the governing equations have been sought were obtained from digital images of cut planes through a glass model. These were produced by laser light sheet illumination, as shown for example in Fig. 1.

A hybrid elliptic-algebraic procedure has been adopted for the generation of the numerical grid, aiming to discretize the physical domain in finite volumes. Two different levels of discretization have been considered in the

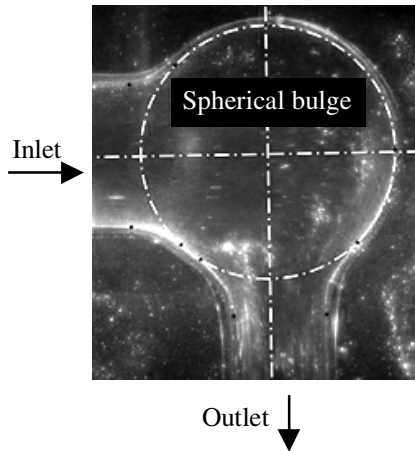


Figure 1 : Digital image of a cut plane through a glass model produced by laser light sheet illumination

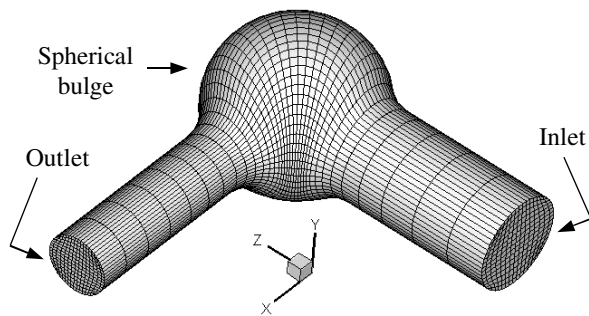


Figure 2 : Geometry of the physical domain and numerical grid (only odd lines of the coarse discretization are shown for clarity)

numerical simulations: coarse ($32 \times 32 \times 70$ grid nodes) and fine ($62 \times 62 \times 138$ grid nodes). Figure 2 illustrates both the numerical grid and the main geometrical details of the physical domain.

For the three-dimensional geometry under consideration, it was possible to produce good quality grids by using the aforementioned procedure. However, grid generation may become a major stumbling block in the extension of this investigation to more complex geometries, such

as those encountered in the study of real aneurysms. A solution may be found in the use of meshless methods [Atluri (2005)], a class of numerical techniques that rely on global interpolation on non-ordered spatial point distributions. Among the various possibilities, the Meshless Local Petrov-Galerkin (MLPG) methods seem to constitute an adequate choice. These have been mainly proposed for elasto-statics [Shen, Han and Atluri (2003)]. Despite this fact and through the MLPG “mixed” approach, Atluri, Han and Rajendran (2004) have developed a meshless finite-volume technique, which is a counterpart to the mesh-based finite-volume method employed throughout this numerical study.

No-slip boundary conditions were applied to all domain surfaces, with the exception of the inlet and outlet sections. At the inlet, a uniform, time-independent w -velocity profile was prescribed. The velocity magnitude was adjusted from case to case according to the desired value of the Reynolds number Re (based on the inlet velocity and diameter) for the simulation. On the other hand, a Sommerfeld radiation condition [Kobayashi, Pereira and Sousa (1993)] was implemented at the outlet section, aiming to minimize undesired wave reflections from this boundary.

If a time-dependent boundary condition is applied to simulate pulsatile inlet flow, further refinement of the time step may be required to resolve the peak accelerations during one oscillation cycle. Shahcheraghi, Dwyer, Cheer, Barakat and Rutaganira (2002) have employed a numerical method similar to the present one (also demanding the solution of a Poisson equation for pressure) with the purpose of simulating three-dimensional pulsatile flow in a human aortic arch. In the foregoing paper the authors have found that a resolution of 360 time steps per cycle was required, which increased computational costs. Nevertheless, convergence problems were not reported therein.

3 Results and discussion

3.1 Steady symmetrical solutions

Initial simulations carried out for increasing values of the Reynolds number in the range 100-300 yielded asymptotically steady solutions of the flow. These are shown in Fig. 3, in terms of in-plane velocity vectors, for the $y - z$ meridional plane of the spherical bulge. The figure portrays purely symmetrical flow patterns with increas-

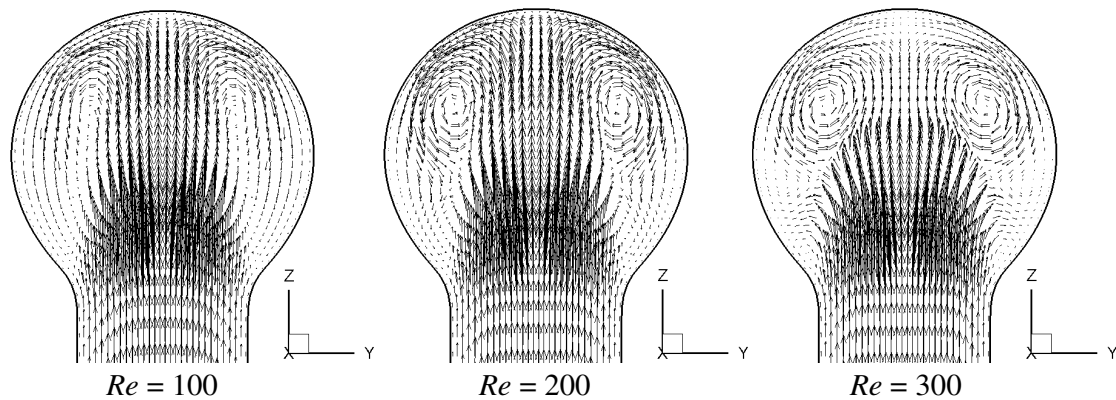


Figure 3 : Steady flow patterns at the $y-z$ meridional plane of the spherical bulge as a function of Reynolds number (velocity vectors have been scaled)

ing complexity. Upon reaching the spherical bulge, the flow separated from the walls, giving rise to the establishment of two large, three-dimensional vortical structures. The fluid in the central region displayed jet-like velocity profiles and it was seen impinging on the wall opposite to the inlet channel. As the Reynolds number increased, the vortical structures occupied a larger area inside the bulge. The strength of these vortices increased with the Reynolds number. However, the velocity of the impinging jet decreased in the sketched plane for $Re = 300$, as a result of a larger out-of-plane jet curvature.

Eventually, the fluid left the spherical bulge by the outlet channel with strong secondary motion. The classical twin-vortex structure encountered in bends was further intensified by existence of the bulge. In addition, despite the action of viscous effects, the reduced section of the outlet channel also acted to increase the angular momentum characterizing secondary motion vortices.

3.2 Time-dependent solution

It was found that the time series obtained for time-dependent flow contained a low-frequency component. Due to the long computational time required for the simulations to cope with a large disparity in time scales, the flow solution presented and discussed in this section has been first obtained employing the coarse grid. Numerical grid independence was investigated by comparing the results produced by coarse and fine spatial discretization, employing the latter for shorter periods of simulation.

The numerical simulations performed for $Re = 400$ did not reach a steady state. In contradistinction to the solutions previously obtained, the v -velocity trace at a

monitor point located in the $x-z$ meridional plane of the spherical bulge displayed long transients of small-amplitude, irregular oscillations, which were violently disrupted by shorter periods of large-amplitude bursts, as shown in Fig. 4. In addition, this figure proves that the symmetry of the flow was broken.

It is undeniable that the intermittence illustrated in Fig. 4 exhibits a certain degree of organization. Namely, the bursts appeared at an approximately constant non-dimensional frequency $\omega = 0.018$. There is an obvious exception to the aforementioned behavior, which occurred at $t \approx 120$.

The characteristic secondary flow pattern previously described for the steady solutions, the so-called Dean vortices, were still present at this higher Reynolds number. However, although during most of the time these vortices exhibited small differences in strength and therefore only a small departure from symmetry in the flow, this topology changed radically when bursting took place.

The event occurring at $t \approx 120$ evidenced the alternating domination of one of the Dean vortices in the flow. This phenomenon, termed as “swirl switching”, has been experimentally observed in turbulent flow through a 90-degree bend [Tunstall and Harvey (1968)]. In that case, it was reported that the flow differs from the classical twin-vortex secondary flow and is an essentially unsteady, bistable flow switching at a low frequency. These two stable configurations were described as mirror images of each other.

Figure 5 substantiates the view above by portraying two instantaneous flow maps recorded at equivalent stages of bursts occurring before and after swirl switch-

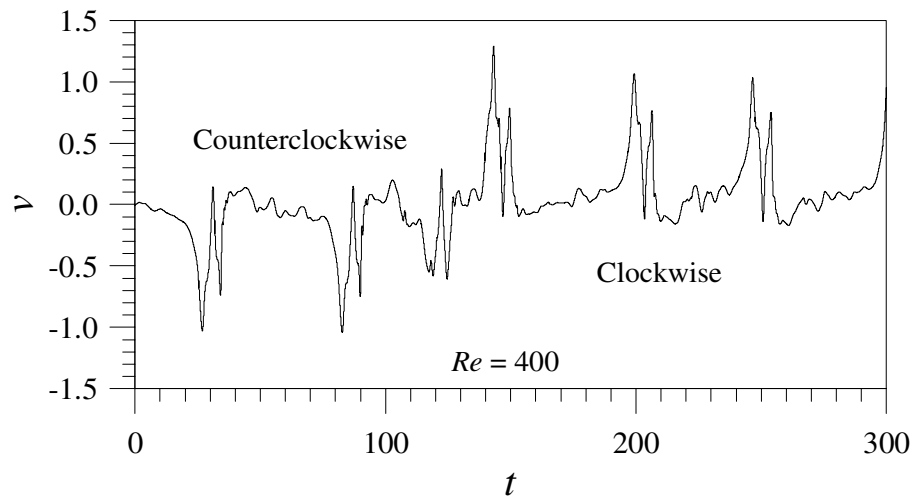


Figure 4 : Time trace of the v -velocity component at a monitor point located in the $x - z$ meridional plane of the spherical bulge for $Re = 400$

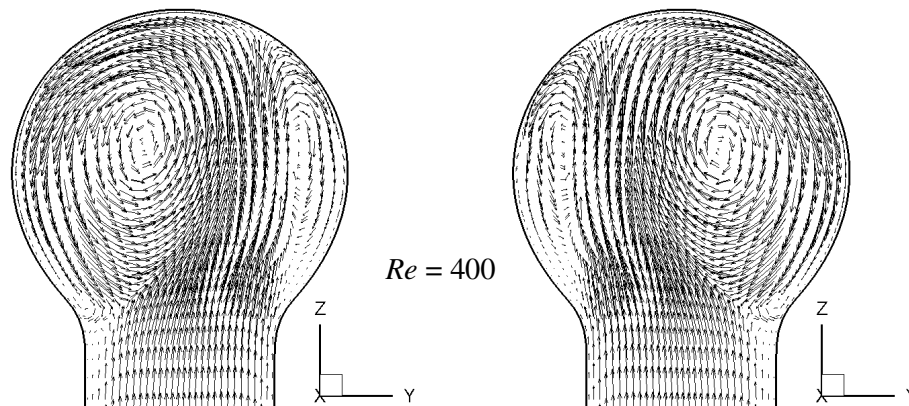


Figure 5 : Instantaneous flow maps at the $y - z$ meridional plane of the spherical bulge for $Re = 400$, before swirl switching (left) and after swirl switching (right)

ing. Referring again to Fig. 4, it can be seen that the counterclockwise-rotating vortex dominated the flow during the first stages. After swirl switching, it was the turn of the clockwise vortex to take over the flow.

Tunstall and Harvey (1968) presumed that separated flow at the inner wall and probably a turbulent flow regime were the necessary conditions for the swirl switching to occur. In the geometry under investigation, flow separation may appear naturally due to the presence of the spherical bulge. Furthermore, the flow at $Re = 400$ shows clearly transitional characteristics, as it will be discussed later. Experimental evidence of the phenomenon for this particular geometry was also given by Mendes, Pinto and

Sousa (2004), although a higher Reynolds number has been considered in the study. Figure 6 illustrates these flow visualization experiments.

Contrary to what one might expect, the mutation from a steady state to a time-dependent behavior did not show, in this case, many similarities with the corresponding change in the flow over a cavity or through a sudden expansion. Namely, the steady symmetry-breaking via supercritical pitchfork bifurcation [Fearn, Mullin and Cliffe (1990)] and the establishment of a time-periodic flow resulting from a Hopf bifurcation [Ghaddar, Korczak, Mikic and Patera (1986); Sobey and Drazin (1986)] were not observed here.

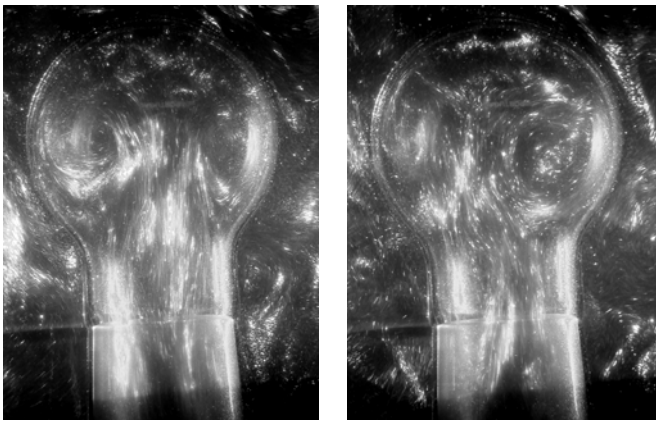


Figure 6 : Experimental flow visualization of swirl switching in the present geometry (compare with Fig. 5)

On the other hand, the low-frequency bursting phenomenon encountered at $Re = 400$ revealed a remarkable resemblance with the oscillatory flow characteristics exhibited by wide-angle diffusers with transitory stall [Rockwell (1983)] and airfoils near stalling conditions [Zaman, McKinzie and Rumsey (1989)]. The typical non-dimensional frequencies ω reported in these studies are in the range 0.01-0.02, as for the present case. In addition, the aforementioned flows have been described to switch abruptly from unstalled to stalled conditions, the latter of these states often corresponding to bursting of a separation bubble.

Cherry, Hillier and Latour (1984) have pointed out that the appearance of low-frequency fluctuations in separation bubbles is a characteristic feature of separated flows in general. Although the origin of this low-frequency motion is not yet fully understood, it has been hypothesized that it may be due to a global instability closely related to an entrained-return flow mechanism [Rockwell (1983)]. Thus, this type of instability essentially manifests itself at the reattachment region of a separated shear layer, giving rise to oscillations which may result from the imbalance between entrained flow and that returned to the separation zone upon reattachment.

Figure 7 depicts the differences between instantaneous flow patterns associated to the period of small-amplitude oscillations and that representative of a bursting event, at the $x-z$ meridional plane. It can be seen that, whereas the former was characterized by the occurrence of an impingement point located nearby the entrance of the outlet channel (arrow in Fig. 7), thereby defining a large recir-

ulation bubble inside the spherical bulge, the latter distinguished itself by the absence of this flow structure. In fact, when a burst took place, the fluid entering the bulge washed out completely the recirculation bubble, thus impinging on the surface opposite to the inlet channel. Taking into account the observed flow features, the global instability mechanism described in the previous paragraphs seems to provide a plausible physical explanation for the low-frequency component displayed in Fig. 4.

An attempt to interpret the events described herein based on the theory of dynamical systems has been made as well. Beginning by postulating that transition from the laminar to the turbulent regime is occurring at $Re = 400$, the following step would be to identify the transition scenario.

Basically four different models describing the route to turbulence [Lichtenberg and Lieberman (1992)] are usually considered: Landau model, Ruelle-Takens-Newhouse model, Feigenbaum model and Pomeau-Manneville model. The flow characteristics observed present a few similarities with the transition to intermittent chaotic behavior explained by the model of Pomeau-Manneville. According to Lichtenberg and Lieberman (1992), intermittent transitions to turbulence have been reported to occur in many experiments. However, they also note that it is not clear that the intermittent transition between two states of a bi-stable system may be described by the Pomeau-Manneville model.

Perhaps a more suitable explanation may be found by considering a different route, termed as “crisis-induced intermittency” by Grebogi, Ott, Romeiras and Yorke (1987). Crises are a common manifestation of chaotic dynamics for dissipative systems, which have also been seen occurring in many experiments and numerical studies. In the present case, intermittency corresponded to the episodic switching between two sustained behaviors, namely bursting and a chaotic orbit between the bursts.

Aiming to determine whether the time-dependent solution really displays a chaotic behavior, a computation of the leading Lyapunov exponent has been carried out for $Re = 400$ using the methodology proposed by Wolf, Swift, Swinney and Vastano (1985). One of the main characteristics of chaotic motion is the strong dependence of the solution on initial conditions. The largest Lyapunov exponent provides a measurement of how unstable a given flow history is. Thus, it carries information about the time scale in which the system becomes unpre-

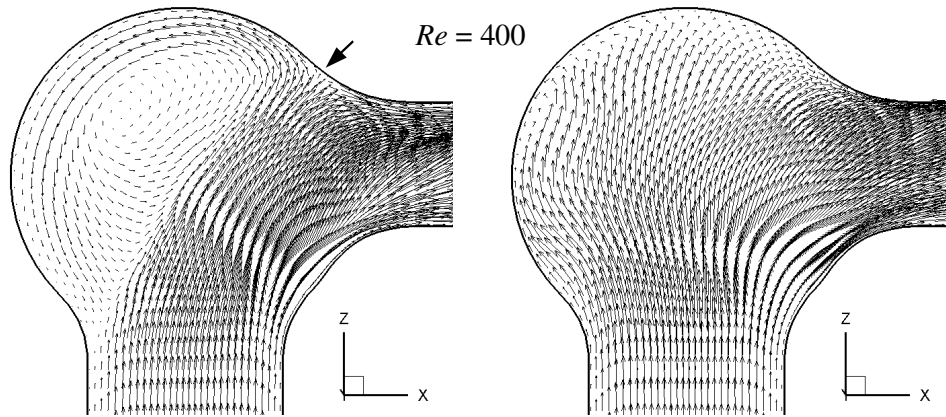


Figure 7 : Instantaneous flow maps at the $x - z$ meridional plane of the spherical bulge for $Re = 400$, depicting small-amplitude oscillations (left) and a bursting event (right)

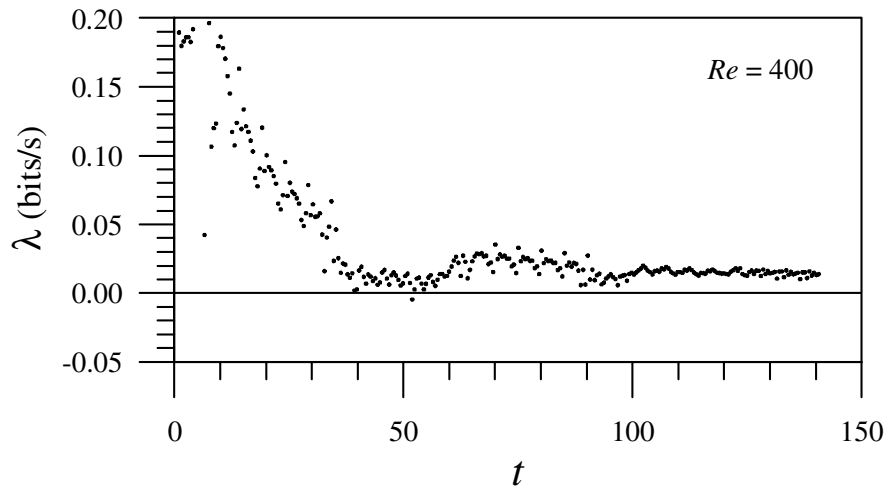


Figure 8 : Temporal convergence of the leading Lyapunov exponent for $Re = 400$

dictable or, in other words, the rate at which the system creates or destroys information.

Figure 8 shows the temporal convergence of the leading Lyapunov exponent. In order to give confidence to this result, besides investigating its stationarity, checks of the exponent estimate were performed as a function of embedding dimension, delay time and evolution time between replacements. The final estimate obtained for this exponent was $\lambda \approx 0.014$ bits/s.

The determination of a positive Lyapunov exponent confirmed the existence of chaotic behavior. In addition, the magnitude of this exponent, expressed in bits of information per second, quantified the divergence of nearby trajectories in phase space. As a basis for a comparison,

the value of the leading Lyapunov exponent characterizing the chaotic state exhibited by the physiological control system described by Mackey and Glass (1977) was $\lambda = 0.0063$ bits/s. Hence, it would take the present flow less than half of the time required by the foregoing system to become unpredictable.

4 Conclusions

Unsteady numerical simulations of the flow through a spherical bulge in a 90-degree asymmetrical bend have been carried out for Reynolds number in the range 100-400. The results obtained have shown that the flow reaches asymptotically steady, symmetrical solutions for Reynolds numbers up to 300.

By contrast, the flow behavior at a Reynolds number value of 400 has shown to be characterized by long transients of small-amplitude, irregular oscillations, which were violently disrupted by shorter periods of large-amplitude bursts. However, such intermittent behavior exhibited an organized pattern, as the bursting events occurred at an approximately constant non-dimensional frequency $\omega = 0.018$.

The low-frequency bursts observed seemed to be due to a global instability closely related to an entrained-return flow mechanism. In addition, it was shown that the striking symmetry-breaking of the flow inside the bulge seen in the time-dependent solution was the result from the alternating domination of one of the Dean vortices, usually termed as swirl switching.

The theory of dynamical systems also helped to interpret the physical behavior of the flow. An explanation for the observed phenomena was found on the occurrence of crisis-induced intermittency. The estimate of the leading Lyapunov exponent computed for the flow was consistent with a transition to intermittent chaotic behavior.

Acknowledgement: The assistance of Mr. P. J. Mendes in the preparation of the experimental flow visualization images is gratefully acknowledged.

References

- Atluri, S. N.** (2005): Methods of Computer Modeling in Engineering & the Sciences, vol. 1, Tech Science.
- Atluri, S. N.; Han, Z. D.; Rajendran, A. M.** (2004): A new implementation of the meshless finite volume method, through the MLPG “mixed” approach, *CMES: Computer Modeling in Engineering & Sciences*, vol. 6, pp. 491-514.
- Berger, S. A.; Jou, L.-D.** (2000): Flows in stenotic vessels, *Annu Rev Fluid Mech*, vol. 32, pp. 347-382.
- Butty, V. D.; Gudjonsson, K.; Buchel, P.; Makhijani, V. B.; Ventikos, Y.; Poulikakos, D.** (2002): Residence times and basins of attraction for a realistic right internal carotid artery with two aneurysms, *Biorheology*, vol. 39, pp. 387-393.
- Cherry, N. J.; Hillier, R.; Latour, M. E. M. P.** (1984): Unsteady measurements in a separated and reattaching flow, *J Fluid Mech*, vol. 144, pp. 13-46.
- Drazin, P. G.** (1999): Flow through a diverging channel: instability and bifurcation, *Fluid Dyn Res*, vol. 24, pp. 321-327.
- Drikakis, D.** (1997): Bifurcation phenomena in incompressible sudden expansion flows, *Phys Fluids*, vol. 9, pp. 76-87.
- Durst, F.; Pereira, J. C. F.; Tropea, C.** (1993): The plane symmetric sudden-expansion flow at low Reynolds numbers, *J Fluid Mech*, vol. 248, pp. 567-581.
- Fearn, R. M.; Mullin, T.; Cliffe, K. A.** (1990): Nonlinear flow phenomena in a symmetric sudden expansion, *J Fluid Mech*, vol. 211, pp. 595-608.
- Ghaddar, N. K.; Korczak, K. Z.; Mikic, B. B.; Patera, A. T.** (1986): Numerical investigation of incompressible flow in grooved channels. Part 1. Stability and self-sustained oscillations, *J Fluid Mech*, vol. 163, pp. 99-127.
- Grebogi, C.; Ott, E.; Romeiras, F.; Yorke, J. A.** (1987): Critical exponents for crisis-induced intermittency, *Phys Rev A*, vol. 36, pp. 5365-5380.
- Hallworth, G. W.; Westmoreland, D. G.** (1987): The twin impinger – A simple device for assessing the delivery of drugs from metered-dose pressurized inhalers, *J Pharm Pharmacol*, vol. 39, pp. 966-972.
- Kobayashi, M. H.; Pereira, J. C. F.; Sousa, J. M. M.** (1993): Comparison of several open boundary numerical treatments for laminar recirculating flows, *Int J Numer Meth Fl*, vol. 16, pp. 403-419.
- Ku, D. N.** (1997): Blood flow in arteries, *Annu Rev Fluid Mech*, vol. 29, pp. 399-434.
- Li, Q.; Shen, S.; Han, Z. D.; Atluri, S. N.** (2003): Application of meshless local Petrov-Galerkin (MLPG) to problems with singularities, and material discontinuities, in 3-D elasticity, *CMES: Computer Modeling in Engineering & Sciences*, vol. 4, pp. 571-586.
- Lichtenberg, A. J.; Lieberman, M. A.** (1992): Regular and Chaotic Dynamics, Springer-Verlag, New York.
- Liou, T. M.; Liou, S. N.** (1999): A review on *in vitro* studies of hemodynamic characteristics in terminal and lateral aneurysm models, *Proceedings of the National Science Council ROC (B)*, vol. 23, pp. 133-148.
- Mackey, M. C.; Glass, L.** (1977): Oscillation and chaos in physiological control systems, *Science*, vol. 197, pp. 287-289.
- Mendes, P. J.; Pinto, J. F.; Sousa, J. M. M.** (2004): Visualization and measurement of the flow through a stan-

dard analyser used for quality control of medical aerosol products. Presented at the 11th International Symposium on Flow Visualization, University of Notre Dame, Indiana.

Mizushima, J.; Okamoto, H.; Yamaguchi, H. (1996): Stability of flow in a channel with a suddenly expanded part, *Phys Fluids*, vol. 8, pp. 2933-2942.

Pereira, J. C. F.; Sousa, J. M. M. (1993): Finite volume calculations of self-sustained oscillations in a grooved channel, *J Comput Phys*, vol. 106, pp. 19-29.

Pereira, J. C. F.; Sousa, J. M. M. (1995): Experimental and numerical investigation of flow oscillations in a rectangular cavity, *J Fluid Eng-T ASME*, vol. 117, pp. 68-74.

Pereira, J. C. F.; Sousa, J. M. M. (1999): Confined vortex breakdown generated by a rotating cone, *J Fluid Mech*, vol. 385, pp. 287-323.

Rockwell, D. (1977): Prediction of oscillation frequencies for unstable flow past cavities, *J Fluid Eng-T ASME*, vol. 99, pp. 294-300.

Rockwell, D. (1983): Oscillations of impinging shear layers, *AIAA J*, vol. 21, pp. 645-664.

Rockwell, D.; Naudascher, E. (1978): Review – Self-sustained oscillations of flows past cavities, *J Fluid Eng-T ASME*, vol. 100, pp. 152-165.

Rockwell, D.; Naudascher, E. (1979): Self-sustained oscillations of impinging free shear layers, *Annu Rev Fluid Mech*, vol. 11, pp. 67-94.

Shahcheraghi, N.; Dwyer, H. A.; Cheer, A. Y.; Barakat, A. I.; Rutaganira, T. (2002): Unsteady and three-dimensional simulation of blood flow in the human aortic arch, *J Biomech Eng-T ASME*, vol. 124, pp.378-387.

Sobey, I. J.; Drazin, P. G. (1986): Bifurcations of two-dimensional channel flows, *J Fluid Mech*, vol. 171, pp. 263-287.

Tunstall, M. J.; Harvey, J. K. (1968): On the effect of a sharp bend in a fully developed turbulent flow, *J Fluid Mech*, vol. 34, pp. 595-608.

Valencia, A. (2004): Flow dynamics in models of intracranial terminal aneurysms, *Mech Chem Biosystems*, vol. 1, pp. 221-231.

Wolf, A.; Swift, J. B.; Swinney, H. L.; Vastano, J. A. (1985): Determining Lyapunov exponents from a time series, *Physica D*, vol. 16, pp. 285-317.

Yip, T. H.; Yu, S. C. M. (2001): Cyclic transition to turbulence in rigid abdominal aortic aneurysm models, *Fluid Dyn Res*, vol. 29, pp. 81-113.

Zaman, K. B. M. Q.; McKinzie, D. J.; Rumsey, C. L. (1989): A natural low-frequency oscillation over airfoils near stalling conditions, *J Fluid Mech*, vol. 202, pp. 403-442.

